Seismic impedance inversion using closed-loop convolutional neural network: An application in turbidite reservoirs

Fábio Júnior Damasceno Fernandes[1,*], Eberton Rodrigues Oliveira Neto[1], Leonardo Teixeira[3], Antonio Fernando Menezes Freire[1,2], Wagner Moreira Lupinacci[1,2], [1]GIECAR-UFF, [2]INCT-GP, [3]Petrobras

This paper was prepared for presentation during the 18th International Congress of the Brazilian Geophysical Society held in Rio de Janeiro, Brazil, 16-19 October 2023.

Abstract

Estimating accurate acoustic impedance models has been an essential routine for reservoir characterization over the last two decades. In most cases, the procedure relies on minimizing an objective function. We presented a deep learning-based approach for seismic impedance inversion using a closed-loop convolutional neural network (CNN). This architecture employs a cycle-consistency loss to learn the context of training data better and produce high-reliable outputs. We trained our network with pseudo-wells simulating intercalations between sandstones, shale, and carbonates. The trained CNN was applied for seismic inversion in the Eocene and Paleocene intervals of the New Jubarte Field, Campos Basin, Brazil. The results show that the CNN-based inverted model presents high resolution and lateral continuity, matching the well-log data with a linear correlation coefficient of 0.75. This deep-learning-based seismic impedance approach performed better than the traditional model-based inversion, indicating that our proposal can be a useful alternative and steadily employed for quantitative seismic interpretation.

Introduction

Acoustic impedance is a crucial parameter for reservoir characterization as it directly correlates to reservoir properties such as porosity, fluid saturation, and facies. The estimation of acoustic impedance from seismic reflection data improves the interpretation and prediction of petroelastic properties. Over the last decades, several methods have been developed to perform deterministic seismic impedance inversion (Russel, 1988; Tarantola, 2005). However, traditional seismic inversion approaches based on the convolutional model suffer from problems like non-linearity, non-uniqueness, and ill-conditioning. In addition, challenges remain due to inherent limitations of the seismic method, such as noise, limited bandwidth, numerical approximations, and physical assumptions in forward modeling (Tarantola, 2005). This results in unstable and uncertain inverted models.

Deep learning is a field of machine learning that employs deep neural networks to learn complex functions from data. Deep-learning routines are used in computer vision, where the networks can extract representative features from data (Goodfellow et al., 2016). Given its versatility, deep learning recently gained popularity in geophysics to solve several tasks such as the identification of faults and horizons (Wu et al., 2019; Vizeu et al., 2022), facies classification (Vizeu et al., 2021), porosity modeling (Allo et al., 2021), and seismic impedance inversion (Biswas et al., 2019; Das et al., 2019; Ge et al., 2022). One of the breakthroughs of deep learning for seismic inversion is the possibility of handling non-linear mapping operators between seismic amplitude data and acoustic impedance without assuming a unique wavelet in the linear convolutional model.

For many years, the multilayer perceptron (MLP) dominated the field of seismic inversion problems using machine learning (Röth and Tarantola, 1994) mainly due to computational limitations of more complex architectures like the convolutional neural network (CNN) for solving large-scale problems. CNNs are more robust than MLPs as they account for local connectivity and are easier to train. However, the lack of training data is a challenging step in deep learning-based methods for seismic inversion. To overcome that, the procedure can include the strategy of creating pseudo-logs of acoustic impedance based on geostatistics and performing the forward modeling through the 1D convolutional model to train the CNNs (Biswas et al., 2019; Ge et al., 2022). The pseudo-wells bring realistic high-resolution information to the inversion process.

The most common approach for seismic impedance inversion using deep learning is by designing a neural network for regression and adopting the mean squared error (MSE) as the loss function to train it. However, the MSE loss only measures the pixel-wise difference between the network output and a given label, disregarding structural differences between the two images, leading to smooth results. As an alternative, Zhu et al. (2017) introduced the cycle-consistency loss for image-to-image translation in the CycleGAN. This loss function overcomes the main limitations of the MSE loss and brings more robustness to seismic inverse problems. The CNN trained with the cycle-consistency loss function is called closed-loop CNN.

Here we perform a seismic impedance inversion using a 1D CNN trained with the cycle-consistency loss function. The closed-loop CNN combines a subnetwork for inversion and another for forward mapping. The model is trained with labeled data from pseudo-wells and unlabeled data randomly extracted from the application dataset. We evaluate the performance of our model for the characterization of turbidite reservoirs of the Eocene and Paleocene in the New Jubarte Field, Campos Basin, Brazil.

Theory and methodology

This section describes the steps to build the training and testing datasets using pseudo-wells. We also explore the architecture of the closed-loop CNN and the training and testing metrics.

Seismic forward modeling

The post-stack convolutional model gives the linear relationship between acoustic impedance and the zero-offset seismic data. A seismic trace can be modeled by the convolution of a wavelet with a reflection coefficient series in the time domain. In turn, the reflection coefficient is the response of the subsurface to the contrasts of acoustic impedance between overlapping layers:

$$r(t) = \frac{z(t+dt) - z(t)}{z(t+dt) + z(t)}, \quad (1)$$

where $z(t+dt)$ and $z(t)$ are the acoustic impedance of the incident and transmitted ray side, respectively. Considering a weak-contrast medium with $r(t) < 0.3$ and discretizing Equation 1 in a uniform grid, a seismic trace d can be written as (Russell, 1988):

$$d = Gm + n, \quad (2)$$

where G is the forward modeling operator, m is the acoustic impedance, and n is noise. We performed the seismic forward modeling of the acoustic impedance models through the convolutional model using different Ricker wavelets with central frequencies varying from 20 to 35 Hz. To make the network robust to noise presence, random noises were applied in the synthetic seismic data with signal-to-noise ratios ranging from 10 to 35 dB.

Synthetic acoustic impedance generation

Dvorkin et al. (2014) describe a workflow to build pseudo-wells that can reproduce common patterns observed in geology such as reservoir properties continuity and vertical facies variation. Initially, a facies log is generated using the first-order Markov chain Monte Carlo (McMC) with a transition matrix T which the term $T_{i,j}$ relates the probability of a given facies i transitioning to another j vertically, depending only on the facies i immediately below. Let the study area be composed of three facies: sandstones, shale, and carbonates. To build the facies log, we used the following matrix T:

$$T = \begin{bmatrix} 0.93 & 0.07 & 0.0 \\ 0.02 & 0.97 & 0.01 \\ 0.05 & 0.10 & 0.85 \end{bmatrix} \quad (3)$$

where the first row $i = 1$ is the probability of all facies being deposited above a sandstone. For example, we have a 0.07 probability of depositing a shale above a sandstone ($T_{1,2} = 0.07$). The second and third rows refer to the shale and carbonates, respectively. For each facies, a spatial-covariance matrix brings the high-frequency information of the variogram to the stochastic simulations, while the statistical measurements carry out the mean and standard deviation. A single simulation is obtained by adding the smooth trend (low-frequency information) to the residual pseudo-log achieved by multiplying the spatial-covariance matrix with a random noise $N(0,1)$ (Figure 1). An infinite number of pseudo-logs of acoustic impedance can be generated through this workflow. It is important to highlight that the facies are used only to bring rock-physics information to the pseudo-well generation step, as they are not utilized in the neural network. The transition matrix shown in Equation 3 was used to generate the facies pseudo-logs of all pseudo-wells. For the exponential variogram model of acoustic impedance, we set random ranges varying from 30 to 100 samples constrained by facies.

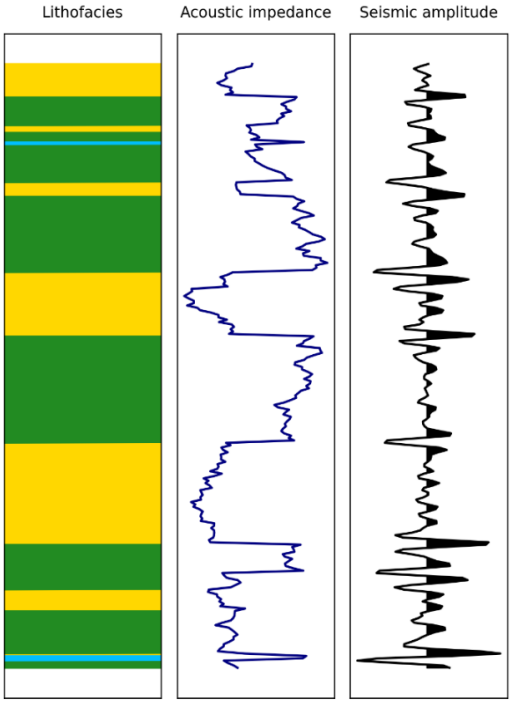

Figure 1 *– Pseudo-well of the training set. The yellow, green, and blue colors represent the sandstones, shale, and carbonates in the lithofacies track.*

Closed-loop convolutional neural network

This study treated the seismic impedance inversion as a pixel-wise regression problem. Therefore, to solve it, we designed a 1D closed-loop CNN composed of two subnetworks with U-Net architecture (Ronneberger et al., 2015). Our U-Net comprises three elements: the encoder, decoder, and skip connections. The encoder consists of repeated two consecutive padded 3x1 convolutional layers followed by batch normalization (BN), hyperbolic tangent activation function (Tanh), and 2x1 max pooling layer with stride 2 for downsampling. This element of U-Net is responsible for learning a hierarchy of features. The decoder is almost symmetrical to the encoder, with 2x1 transposed convolutions with stride for upsampling, a skip connection, and two consecutive padded 3x1 convolutions followed by BN and Tanh. The last layer is a 1x1 convolutional that outputs a vector with the same size as the input. The decoder and skip connections decode information to get precise predictions.

The closed-loop CNN architecture consists of training the inversion subnetwork to estimate the acoustic impedance

taking the seismic amplitude data as input. On the other hand, the forward subnetwork aims to approximate the seismic forward modeling using the acoustic impedance (Figure 2). We built the closed-loop CNN using the PyTorch framework version 1.13.

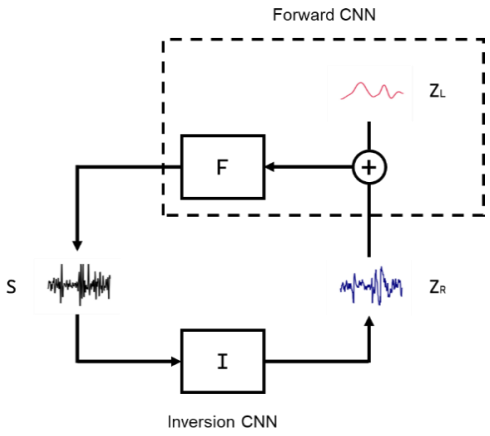

Figure 2 *– Architecture of the closed-loop CNN. Z_R is the output of the Inversion CNN (I) with an input S. Z_R is summed to the low-frequency information Z_L and fed to the Forward CNN (F).*

Cycle-consistency loss function

Zhu et al. (2017) proposed the cycle-consistency loss for image-to-image translation in the CycleGAN. This loss function presents several advantages over the simple MSE loss: unneeded use of paired data for the whole training set; preservation of image content when translating from input to output domain; guarantees that an input image translated to output domain and back again is consistent; robustness to image variations; capture of semantic information such as shapes and identities. This leads to a semi-supervised learning problem. Considering only the inversion network, the loss function of the open-loop network is given by the MSE of:

$$J_o^1(\theta_I) = \frac{1}{N}\left\|m - F_{\theta_I}(d)\right\|_2^2, \tag{4}$$

where d is the input seismic data labeled by the output acoustic impedance m, forming N pairs of training samples. By minimizing the loss function of the inversion network, the parameters θ_I are updated. The function F_{θ_I} is responsible for performing the seismic inversion. It is straightforward that the loss function of the open-loop network for forward modeling follows the same behavior:

$$J_o^2(\theta_F) = \frac{1}{N}\left\|d - F_{\theta_F}(m)\right\|_2^2. \tag{5}$$

These two loss functions are used in the closed-loop CNN to calculate the cycle-consistency loss, expressed as:

$$\begin{aligned} J_C(\theta_F, \theta_I) = {} & \beta_1\left(J_o^1(\theta_I) + J_o^2(\theta_F)\right) \\ & + \beta_2\left(J_{cycle}^1(\theta_I, \theta_F)\right. \\ & \left. + J_{cycle}^2(\theta_I, \theta_F)\right) \\ & + \beta_3 J_{cycle}^3(\theta_I, \theta_F), \end{aligned} \tag{6}$$

where

$$J_{cycle}^1(\theta_F, \theta_I) = \frac{1}{N}\left\|d - F_{\theta_F}(F_{\theta_I}(d))\right\|_2^2, \tag{7}$$

$$J_{cycle}^2(\theta_F, \theta_I) = \frac{1}{N}\left\|m - F_{\theta_I}(F_{\theta_F}(m))\right\|_2^2, \tag{8}$$

$$J_{cycle}^3(\theta_F, \theta_I) = \frac{1}{N^*}\left\|d^* - F_{\theta_F}(F_{\theta_I}(d^*))\right\|_2^2, \tag{9}$$

with J_{cycle}^1 and J_{cycle}^2 corresponding to the cyclic losses concerning the labeled seismic amplitude data and acoustic impedance, respectively. In addition, the cycle-consistency loss takes the loss J_{cycle}^3 concerning unlabeled data d^*, which makes this a semi-supervised training. The hyperparameters β_1, β_2, and β_3 are used for tuning the components of the cycle-consistency loss.

Training and testing step

We trained the 1D closed-loop CNN for 500 epochs using the Adam optimizer (Kingma and Ba, 2014) and the cycle-consistency loss (Zhu et al., 2017). The training and test dataset consists of 3200 and 800 labeled pseudo-wells, respectively. The unlabeled data comprises 3200 pairs of seismic amplitude and low-frequency acoustic impedance randomly extracted from the 3D seismic volume of the application set. The batch size selected for training was 128 and the learning rate is 0.001. Cycle-consistency loss parameters β_1, β_2, and β_3 were set to 1, 10, and 1, respectively. Training, testing, and application were performed using an NVIDIA GeForce RTX 3060 GPU Figure 3 shows the train and test losses of the closed-loop CNN over the 500 epochs. The network converged after approximately 50 iterations, with the train and test losses almost equal. We decided to adopt the parameters of epoch 100 to avoid overfitting effects found after the last iteration.

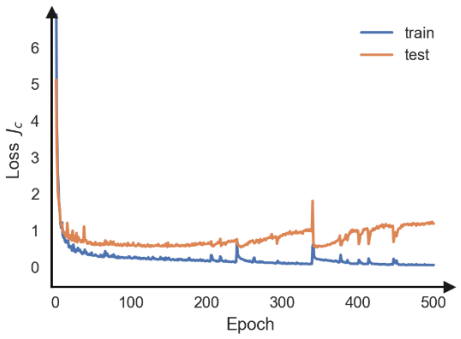

Figure 3 *– Train and test losses by epoch.*

Figure 4 illustrates an example of the inversion result in a pseudo-well of the test set. The inversion and forward subnetwork learned in the closed-loop how to map from amplitude to acoustic impedance domain and vice-versa. There is also a high-resolution content in the inverted acoustic impedance that would be lost if adopting the simple MSE instead of the cycle-consistency loss.

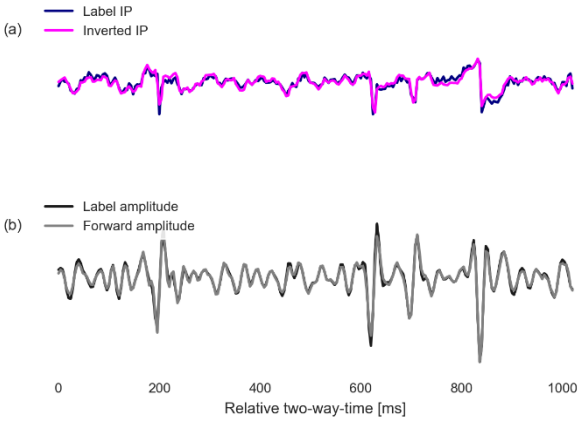

Figure 4 *– Application of the closed-loop CNN in a pseudo-well of the test set for (a) inversion and its respective (b) forward modeling.*

Application

We evaluate the network for seismic impedance inversion in the Eocene and Paleocene intervals of the New Jubarte Field, Campos Basin, Brazil. Shale, marls, and turbidite sandstones form this section. The turbidite reservoirs of the Carapebus Formation are composed of clean sands with high-porosity characteristics (Winter et al., 2007). Regarding the acoustic impedance, Fernandes et al. (2022) observe strong overlaps of the sandstones and shale in well-log data, representing a challenge for their identification.

The seismic inversion was performed in the time domain. With the wells tied with seismic data and the Eocene and Paleocene horizons mapped, we built the low-frequency model of acoustic impedance using ordinary kriging guided by the seismic horizons. The well 6-BRSA-497-ESS was chosen as the blind test, not being used to build the low-frequency model. For convenience, we will refer to it as Well A. After the inversion, this low-frequency model is added to the network output and denormalized to reach the absolute acoustic impedance values.

The result of the seismic impedance inversion using the inversion subnetwork is illustrated in Figure 5. In general, we observe a high vertical resolution and good lateral continuity. The targets are two occurrences of the Carapebus Formation: a 46-m thick layer ranging from 3133-3170ms and a 34-m thick layer in the interval of 3277-3306ms. We observe a strong correlation between the inversion result and the acoustic impedance log of Well A, matching the values of both target reservoirs (from yellow to green tones). A non-reservoir interval (the Ubatuba Formation) occurs between the upper and lower Carapebus Formation, marked by intermediate-to-high acoustic impedance associated with shale. Above the upper Carapebus Formation, the inversion shows a third thick interval with low acoustic impedance values, possibly related to another turbidite reservoir. The well-log data reaches this region, but the caliper log indicates break-up zones, compromising the analysis. Despite that, the composite log facies indicate intercalations of sandstone and marls between 3028-3054ms, highlighting a possible reservoir zone.

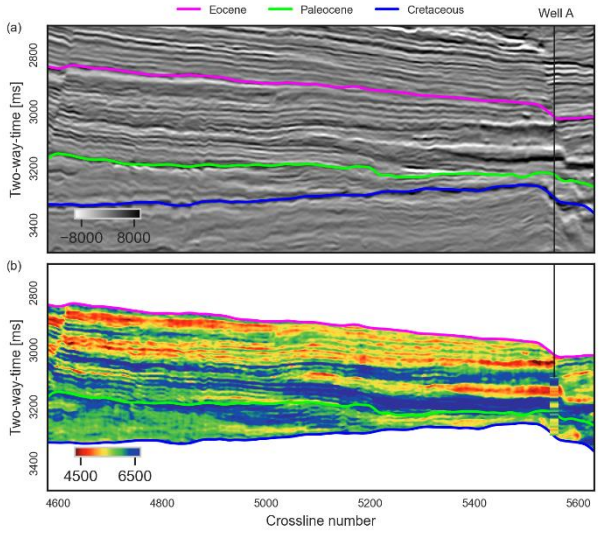

Figure 5 *– Deep learning-based (b) seismic impedance inversion at the (a) seismic section crossing Well A.*

There are slight differences in the values of observed seismic and the forward modeling of the inversion achieved through the forward subnetwork (Figure 6). Despite that, the forward subnetwork learned to map from acoustic impedance to amplitude domain, preserving all features found on observed seismic data. This was crucial to the functioning of the closed-loop network and, furthermore, we can adopt this trained subnetwork in other applications to perform seismic forward modeling with a non-linear mapping operator.

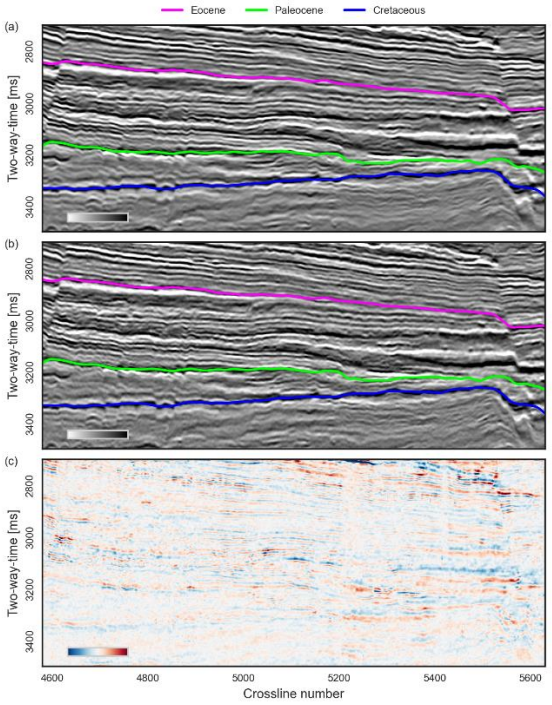

Figure 6 *– Comparison between (a) seismic amplitude data and (b) the result of the forward modeling of inversion results using the forward subnetwork. In (c), it is shown the difference between (a) and (b).*

Discussion

The seismic impedance inversion with the proposed deep learning-based method presents a high-frequency content that allows the identification of thin-layered intervals. The high-resolution content of our approach can be linked to the geostatistics information introduced on the pseudo-well generation via variogram and the cycle-consistency loss. By adopting a more straightforward loss function like the MSE in an open-loop CNN, most high-frequency information would be lost as it disregards the context, merely calculating the pixel-wise difference between labeled and inverted acoustic impedance data. Our proposal is extensible to pre-stack inversion, as rock-physics models and the seismic amplitude by the angle-dependent Zoeprittz equations can also generate the pseudo-wells. Furthermore, the inversion can be achieved in depth since no assumption is made on deep learning-based methods regarding the seismic domain.

A disadvantage of the 1D CNN resides in the lack of local lateral continuity. Despite that, this effect is negligible compared to other results of deep learning-based seismic inversion found in the literature (Zhang et al., 2022; Sun et al., 2023), highlighting the robustness of our approach. Ge et al. (2022) also reached good inversion results using the same 1D closed-loop CNN architecture. We presume that 2D network architectures can improve lateral continuity and preserve high-resolution information, possibly producing better models because the network will account for lateral connectivity. However, creating 2D synthetic seismic data is more challenging than in the 1D scenario. Authors such as Wu et al. (2019) and Vizeu et al. (2022) present approaches for 2D and 3D synthetic seismic data generation that can produce a large variety of structures like faults and folds and elastic properties like acoustic impedance. However, they used the models for other purposes instead of seismic inversion. Although, it is straightforward that the computational cost will increase in the 2D case. For example, our network has 21,767,554 trainable parameters, while a simple extension of the same architecture in 2D has 62,204,034. This leads to a significant increase in computational time.

Historically, deep-learning algorithms were essentially data-driven in the field of computer vision. However, computer vision is a data-rich domain, which differs from seismic inversion, where data is scarce. Thus, parallel to creating high-quality synthetic data, scholars attempt to bring physics knowledge to the deep learning-based seismic inversion (Lin et al., 2023). Our approach is within this field, as the forward subnetwork approximates the physical principles of translating from the acoustic impedance to the seismic amplitude domain. This architecture is called a physics-guided neural network (PGNN). Another possible strategy is adopting a physics-informed neural network (PINN). The PINN uses a known physics rule, such as the convolutional model, to perform the forward mapping, combining the output to calculate the loss function. Future research can compare PINN and PGNN for seismic impedance inversion.

Closed-loop CNN versus model-based inversion

A comparison between our approach for seismic inversion and the traditional model-based inversion (Russell, 1988) is presented in Figure 7. The parametrization for the Tikhonov damping was set to 0.6 as the model-based inversion performed with this value reached the highest correlation coefficient with Well A, maintaining a geological consistency. We highlight a similar vertical resolution of deep learning-based and model-based inversions. Nevertheless, the CNN-based inversion shows a lower influence of the low-frequency model. This is a key factor because the wells are often drilled at large distances from each other and in a few amounts, representing a challenge for constructing the low-frequency model using interpolation methods. The model-based inversion is more sensitive to the low-frequency model as it iteratively updates it until matching some tolerance or number of iterations. In the model-based inversion, the visual correlation between inversion and well-log data is worse than in the CNN-based inversion. A negative aspect is that our inversion proposal often presents some non-geological vertical artifacts not observed in the model-based approach. We suggest that improvements in the network architecture and training data can overcome this unwanted behavior.

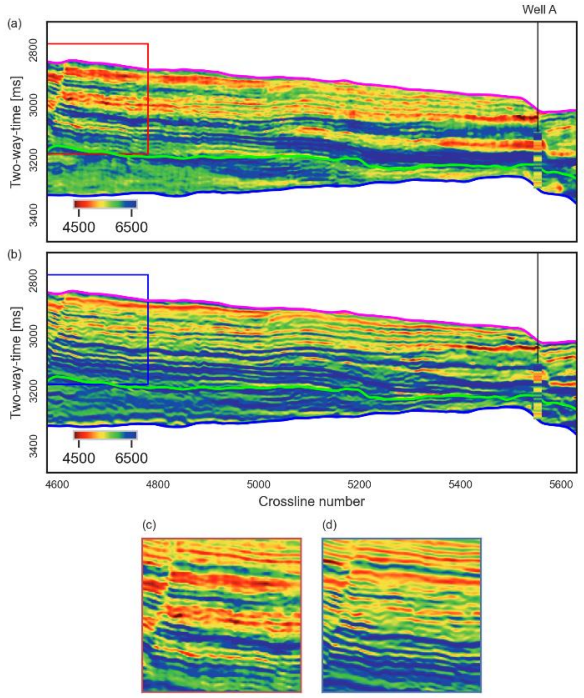

***Figure 7** – Comparison between (a) deep learning-based seismic impedance inversion and (b) traditional model-based inversion. In (c) and (d), zooms are shown in the red and blue boxes, respectively.*

Quantitatively, the CNN inversion reached the highest correlation coefficient and lowest dispersion compared to the acoustic impedance log of Well A (Figure 8). The Pearson linear correlation coefficient and mean absolute percentage error of the deep learning-based method are 0.75 and 0.07, respectively, whereas, in the model-based inversion, these estimates are 0.58 and 0.10, respectively. Restricting the analysis to the reservoir zones, the CNN-based inversion also shows a better prediction of the acoustic impedance log,

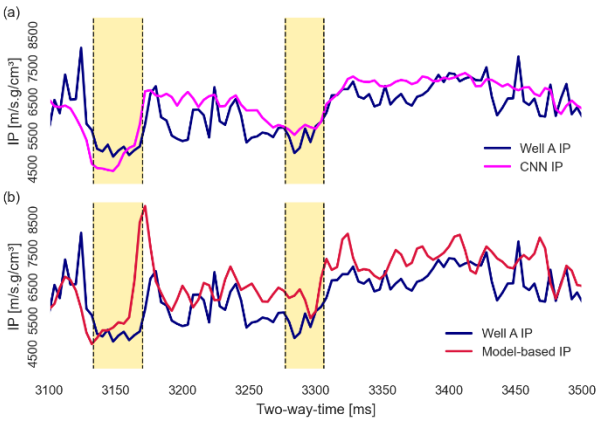

***Figure 8** – Comparison between the acoustic impedance log of Well with (a) deep learning-based inversion and (b) model-based inversion. The reservoirs of the Carapebus Formation are the yellow intervals.*

Conclusions

We presented a deep learning-based method to perform the seismic impedance inversion. The closed-loop CNN employs the cycle-consistency loss function to preserve features when translating from acoustic impedance to seismic amplitude domains and back again. An application in a turbidite reservoir proves the potential of our approach, reaching a high-resolution acoustic impedance model with good lateral continuity. The CNN-based had a better quantitative and qualitative performance compared to the model-based inversion, achieving a correlation coefficient of 0.75 in Well A. Deep learning-based seismic inversion is a topic that is gaining considerable attention from researchers, and we endorse that promising results like this indicate that they soon can be fully incorporated into reservoir characterization.

Acknowledgments

The authors thank Petrobras for financing the R&D project, ANP for providing data used in this research, and INCT-GP/CNPq for supporting this research.

References

Allo, F., et al., 2021. Characterization of a carbonate geothermal reservoir using rock-physics-guided deep neural networks. The Leading Edge, 40(10), 751-758.

Biswas, R., Sen, M.K., Das, V., Mukerji, T., 2019. Prestack and poststack inversion using a physics-guided convolutional neural network. Interpretation, 7(3), SE161-SE174.

Das, V., Pollack, A., Wollner, U., Mukerji, T., 2019. Convolutional neural network for seismic impedance inversion. Geophysics, 84(6), R869-R880.

Dvorkin, J., Gutierrez, M.A., Grana, D., 2014. Seismic reflections of rock properties. Cambridge University Press.

Fernandes, F.J.D., Freire, A.F.M., Lupinacci, W.M., 2022. Estudo de viabilidade para a classificação Bayesiana em reservatórios turbidíticos do Eoceno no Novo Campo de Jubarte, Bacia de Campos. In: IX SimBGf. Paraná, Brazil.

Ge, Q., et al., 2022. High-resolution seismic impedance inversion integrating the closed-loop convolutional neural network and geostatistics: an application to the thin interbedded reservoir. Journal of Geophysics and Engineering, 19(3), 550-561.

Goodfellow, I., Bengio, Y., Courville, A., 2016. Deep Learning. Adaptive Computation and Machine Learning. Cambridge, Massachusetts: The MIT Press.

Kingma, D.P., Ba, J., 2014. Adam: A method for stochastic optimization. arXiv preprint arXiv:1412.6980.

Lin, Y., Theiler, J., Wohlberg, B., 2023. Physics-Guided Data-Driven Seismic Inversion: Recent progress and future opportunities in full-waveform inversion. IEEE Signal Processing Magazine, 40(1), 115-133.

Ronneberger, O., Fischer, P., Brox, T., 2015. U-Net: Convolutional networks for biomedical image segmentation. In: Medical Image Computing and Computer-Assisted Intervention–MICCAI 2015: 18th International Conference, Munich, Germany, October 5-9, 2015, Proceedings, Part III 18 (pp. 234-241). Springer International Publishing.

Röth, G., Tarantola, A., 1994. Neural networks and inversion of seismic data. Journal of Geophysical Research: Solid Earth, 99(B4), 6753-6768.

Russell, B.H., 1988. Introduction to seismic inversion methods (No. 2). SEG Books.

Sun, J., et al., 2023. Intelligent AVA Inversion Using a Convolution Neural Network Trained with Pseudo-Well Datasets. Surveys in Geophysics, 1-31.

Tarantola, A., 2005. Inverse problem theory and methods for model parameter estimation. SIAM.

Vizeu, F., Neto, E.O., Freire, A.F.M., Lupinacci, W.M., 2021. Convolutional Neural Network for Prediction of Igneous Seismic Facies in the Santos Basin Pre-Salt. In: Second EAGE Conference on Pre-Salt Reservoir (Vol. 2021, No. 1, pp. 1-5).

Vizeu, F., et al., 2022. Synthetic seismic data generation for automated AI-based procedures with an example application to high-resolution interpretation. The Leading Edge, 41(6), 392-399.

Winter, W.R., Jahnert, R.J., França, A.B., 2007. Bacia de Campos. Boletim de Geociências da Petrobras, 15 (2):511-529.

Wu, X., Liang, L., Shi, Y., Fomel, S., 2019. FaultSeg3D: Using synthetic data sets to train an end-to-end convolutional neural network for 3D seismic fault segmentation. Geophysics, 84(3), IM35-IM45.

Zhang, S.B., Si, H.J., Wu, X.M., Yan, S.S., 2022. A comparison of deep learning methods for seismic impedance inversion. Petroleum Science, 19(3), 1019-1030.

Zhu, J.Y., Park, T., Isola, P., Efros, A.A., 2017. Unpaired image-to-image translation using cycle-consistent adversarial networks. In: Proceedings of the IEEE international conference on computer vision (pp. 2223-2232).